

Chromatin Fibers Observed In Situ in Frozen Hydrated Sections. Native Fiber Diameter Is Not Correlated with Nucleosome Repeat Length

C. L. Woodcock

Biology Department, University of Massachusetts, Amherst, Massachusetts 01003

Abstract. Chromatin fibers have been observed and measured in frozen hydrated sections of three types of cell (chicken erythrocytes and sperm of *Patiria miniata* and *Thyone briareus*) representing an ~ 20 -bp range of nucleosomal repeat lengths. For sperm of the starfish *P. miniata*, it was possible to obtain images of chromatin fibers from cells that were swimming in seawater up to the moment of cryo-immobilization, thus providing a record of the native morphology of the chromatin of these cells. Glutaraldehyde fixation produced no significant changes in the ultrastructure or diameter of chromatin fibers, and fiber diameters observed in cryosections were similar to those recorded after low temperature embedding in Lowicryl K11M. Chromatin fiber diameters measured from

cryosections of the three types of nuclei were similar, a striking contrast to the situation for chromatin isolated from these cell types, where a strong positive correlation between diameter and nucleosomal repeat length has been established.

The demonstration of chromatin fibers in unfixed whole cells establishes an unequivocal baseline for the study of native chromatin and chromosome architecture. The significant differences between chromatin fibers in nucleo and after isolation supports a previous observation (P. J. Giannasca, R. A. Horowitz, and C. L. Woodcock. 1993. *J. Cell Sci.* 105:551-561), and suggests that structural studies on isolated material should be interpreted with caution until the changes that accompany chromatin isolation are understood.

EUKARYOTIC chromatin exists in a number of different conformational states. During interphase, there is a range of compaction levels that is roughly correlated with transcriptional competence, and mitosis and meiosis are marked by the transition to chromosomes. How the fundamental units of eukaryotic chromatin, the nucleosome-linker DNA repeats (van Holde, 1988), are modulated to achieve these different states remains a major challenge in understanding nuclear structure and function. Previous experimental approaches to these questions have been concentrated on conventional thin sectioning of nuclei and chromosomes, and on studies of isolated chromatin, neither of which can be relied upon to preserve the native state of chromatin organization. The loss of native structures during chromatin isolation has recently been documented (Giannasca et al., 1993), and the extensive processing necessary to prepare conventional thin sections alters chromatin structures (Langmore and Paulson, 1983). Without a definitive "baseline" for native nuclear organization at the nucleosomal level, it has been impossible to proceed to definitive studies of the higher order chromatin structures.

An approach to native ultrastructure that avoids the problems mentioned above is to vitrify living cells, obtain cryosections, and examine them in the frozen hydrated state (Dubochet et al., 1988). The results can be compared to those obtained with more conventional techniques, providing a qualitative and quantitative assessment of their fidelity. In this communication, cryoelectron microscopy is used to visualize chromatin in unfixed, unstained whole cells. The nuclei selected for cryosectioning have been extensively studied by conventional methods, and shown to contain chromatin in the "30-nm fiber" conformation.

The 30-nm fiber illustrates the difficulty encountered in defining the native state of chromatin. Only in a few nuclei, such as avian erythrocytes and echinoderm sperm, are chromatin fibers seen in thin sections. These nuclei share features such as transcriptional inactivity, low amounts of non-histone chromosomal protein, and long nucleosomal linker DNA (van Holde, 1988). In contrast, the "typical" eukaryotic nucleus contains chromatin in different compaction states, but well-defined 30-nm fibers are usually absent. Nevertheless, chromatin isolated from such nuclei assumes a 30-nm fiber configuration under appropriate ionic conditions (e.g., Thoma et al., 1979; van Holde, 1988). There are also conditions under which the chromatin of interphase nuclei (Kirschner et al., 1977) and mitotic chromosomes (Bahr, 1977; Rattner

Address all correspondence to C. L. Woodcock, Department of Biology, University of Massachusetts, Amherst, MA 01003.

and Hamkalo, 1978) appears as fibers. These conditions usually involve a brief exposure to low ionic strength, such as spreading on a water surface. What, then is the native chromatin organization of the typical interphase nucleus and mitotic chromosome? It can be argued that a 30-nm fiber structure exists, but is not revealed in thin sections because of preparative deficiencies; or, alternatively, that a 30-nm organization is not native, but induced by low ionic strength or during chromatin isolation. MacDowall et al. (1986), observing no higher order chromatin structures in cryosections of cultured cells at metaphase, suggested a liquid organization in which individual nucleosomes had considerable freedom of movement rather than being confined within a fiber. These authors did not, however, examine cryosections of nuclei in which 30-nm chromatin fibers are observed in conventional thin sections.

In the present study, it is shown that chromatin fibers can be observed in cryosections of nuclei from two species of echinoderm sperm and from chicken erythrocytes. This provides an opportunity to measure the diameters of chromatin fibers that have not been exposed to fixatives or dehydrating agents, nor exposed to the changes in ionic milieu required for isolation. The issue of chromatin fiber diameter, and its relationship to nucleosomal repeat has become an important factor in models of fiber architecture: models in which linker DNA is extended and traverses the fiber predict a positive linear relationship between diameter and linker DNA length (Felsenfeld and McGhee, 1986; Williams et al., 1986; Bordas et al., 1986; Athey et al., 1990). The results presented here show that a 20-bp range of nucleosomal spacing does not lead to a significant difference in the diameter of chromatin fibers observed in frozen hydrated sections.

Materials and Methods

Patiria miniata (starfish) were obtained from Marinus Inc. (Long Beach, CA), and *Thyone briareus* (sea cucumber) from Woods Hole Marine Station (Woods Hole, MA). Both were maintained in artificial seawater (ASW)¹ at 12°–14°C. Testes were removed from ripe males and shaken vigorously in ASW, whereupon swimming sperm were released spontaneously. Sperm were concentrated into a paste-like pellet by brief centrifugation, and the supernatant carefully drained. Small samples of the pellets, ~3 μ l in volume were applied to the tips of hollow-cone aluminum specimen pins, and plunged into liquid ethane at -170°C (KF80 freezing apparatus; Leica Inc., Deerfield, IL). Ultra-thin sections were obtained using the FC4 cryo accessory and Ultracut E microtome (Leica Inc.) and a diamond knife with 35° angle (Diatome Inc., Fort Washington, PA). The knife, specimen, and chamber temperature was set at -160°C, and the cutting thickness was nominally 50 nm. Actual section thickness, as measured from stereo pairs, was typically 70 to 100 nm. Sections were transferred to carbon-coated 600-mesh grids, and stored under liquid nitrogen.

Other treatments of the live sperm were as follows: addition of dextran (42 kD; Sigma Chemical Co., St. Louis, MO) to 15 or 20% as a cryoprotectant prior to concentration and freezing; fixation by the addition of glutaraldehyde to 2% for 2 h on ice, followed by washing in ASW; mild homogenization to break off the sperm tails, followed by resuspension in 150 mM NaCl, 15 mM Hepes, pH 8.0. Cells treated with Hepes-NaCl were subsequently processed with the same variations as for the live cells, including fixation and cryoprotection. Aliquots of samples treated with glutaraldehyde were post-fixed with osmium tetroxide and embedded in epoxy resin using standard procedures.

Chicken erythrocytes were frozen as packed pellets of fresh blood, and, also immediately after nuclear isolation and resuspension in 20 mM NaCl, 15 mM Hepes, pH 8.0, as described (Horowitz et al., 1990).

1. *Abbreviations used in this paper:* ASW, artificial seawater; GA, glutaraldehyde.

Cryosections were transferred under liquid nitrogen to a cryoholder (model 626; Gatan Inc., Warrendale, PA) and observed in a Philips CM12 electron microscope operated at 80KV. Minimal dose techniques were used for recording micrographs. Two or more levels of focus (usually 2.0 and 4.0 μ m underfocus) were recorded for each area, and in some cases a second set of micrographs tilted at 10° was obtained. To assess the state of water in the sections, electron diffraction patterns were routinely recorded. The film used was SO-163 (Kodak Inc.), developed for 12 min in D19 (Kodak Inc.). Magnifications were calibrated with a cross-grating replica.

Chromatin fiber diameters were taken from enlargements with a total magnification of 60,000 to 100,000 \times using a 10 \times measuring loupe with 0.1-mm divisions. Measurements were restricted to stretches of fiber that were straight and had a consistent diameter for at least 150 nm. Also recorded for each fiber segment was the angle with respect to the cutting direction (determined from the knife marks). For each data set, the mean, standard deviation, and confidence intervals for the mean were calculated. To test the reliability of the diameter measurements, a set of micrographs was analyzed independently by two observers. The mean diameters differed by only 0.8 nm, and the standard deviations by 0.3 nm, indicating that neither personal bias in selecting fiber "edges" nor an inherent lack of measuring accuracy was affecting the results.

Digitization of negatives was carried out using a TV camera (model C2400; Hamamatsu) interfaced with a Megavision 1024XM image acquisition and display system. A pixel included a 15.3- μ m² area of negative. Power spectra of selected image areas were computed using the SPIDER software system (Frank et al., 1981).

Results

For the study of chromatin in the frozen hydrated state, three well-characterized sources representing an ~20-bp range of nucleosome repeat length were chosen. Chicken erythrocyte nuclei have a nucleosomal spacing of ~212 bp (van Holde, 1988), sperm nuclei from the starfish *Patiria miniata* an ~222-bp repeat length (Giannasca et al., 1993), and a second echinoderm sperm source, the sea cucumber *Thyone briareus*, an ~232-bp repeat (Williams et al., 1986). Chromatin fibers have been isolated from all three following nuclease digestion (van Holde, 1988; Woodcock et al., 1984; Williams et al., 1986; Giannasca et al., 1993), and have also been observed in situ in the nucleus (Davies et al., 1974; Tilney, 1976; Horowitz et al., 1990; Giannasca et al., 1993).

For each source, freezings were made of the native cells, and after treatments shown previously to promote the separation chromatin fibers without affecting their diameter (Horowitz et al., 1990; Giannasca et al., 1993). Also, the effects of glutaraldehyde (GA) fixation were examined and aliquots of fixed material embedded in epoxy resin.

Freezing Conditions and Image Quality

An essential pre-requisite for cryosectioning is freezing of the sample such that ice crystal effects are avoided. In most cases, a cryoprotectant with low osmotic potential (dextran, 40 kD) was added to the suspension prior to freezing. This, in combination with plunging into liquid ethane at -170°C, allowed the vitreous state to be achieved reliably to a depth of several micrometers. Electron diffraction patterns of vitreous material (Fig. 1 a) show a strong, broad ring originating from a spacing of ~0.37 nm, and a weaker ring at ~0.21 nm (Dubochet et al., 1988). Sometimes, a pair of sharper rings at 0.37 and 0.22 nm indicative of cubic ice (Dubochet et al., 1988) were superimposed on the vitreous pattern (Fig. 1 b). Sections with this pattern showed no signs of the microcrystalline structure associated with extensive cubic ice (Dubochet et al., 1988). Sections with electron diffraction

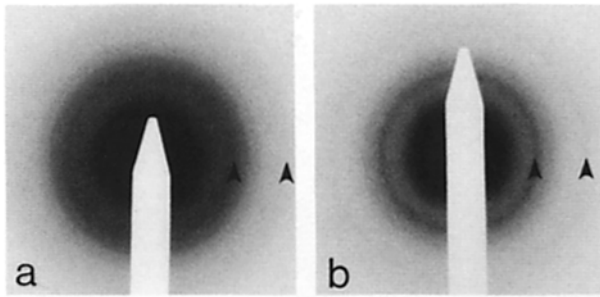


Figure 1. Electron diffraction patterns obtained from cryosections. (a) The pattern typical of vitreous ice with two diffuse rings (arrowheads) corresponding to spacings of 0.37 and 0.21 nm. (b) A pattern with some contribution from cubic ice as seen from the sharper rings (arrowheads) corresponding to spacings of 0.37 and 0.22 nm.

patterns diagnostic of hexagonal ice (Dubochet et al., 1988) were discarded.

Unstained frozen hydrated sections have little inherent amplitude contrast, but phase contrast is obtained in underfocussed images (Stewart, 1989). Initial studies concentrating on the microtubules of the sperm axoneme showed that the microtubules became visible at a nominal defocus of 2 μm , and at 4 μm underfocus, contrast was optimal (Fig. 2). The power spectrum obtained from the Fourier transform of a selected longitudinal section of axoneme shows a prominent layer line at 1/8.8 nm at both underfocus settings (Fig. 2, insets). A similar strong layer line at 1/8.3 nm was noted by Murray (1986) in frozen hydrated whole axonemes from sea urchin sperm. It is clear from the power spectra in Fig. 2 that information is present to at least 5-nm resolution at 4 μm underfocus. The calculated phase contrast transfer function (Erikson and Klug, 1971) for the instrument conditions used in these studies gives a value of ~ 4 nm for the first minimum at a defocus of 4 μm . The effect of defocus on linear measurements of image features were also investigated (see below). These considerations suggest that by routinely collecting images at 2 and 4 μm defocus for each specimen

area, information pertinent to the distribution of nucleosomes (11-nm diam, 5.5-nm thick) would be retained.

Chromatin Fibers Can Be Seen in Frozen Hydrated Sections

Fig. 3 a shows a frozen hydrated section of *T. briareus* sperm exposed to 150 mM NaCl, 15 mM Hepes, pH 8.0 (Giannasca et al., 1993), and dextran cryoprotectant but not fixed. For comparison, the same material after GA fixation and conventional epoxy embedding is shown in Fig. 3 b. Both the frozen hydrated and conventionally prepared cells have nuclei filled with chromatin fibers, and, in general, features seen in the epoxy sections have a similar morphology to those present in the frozen material. When cells were fixed with glutaraldehyde after Hepes-NaCl and then frozen, they appeared identical to the unfixed cells (not shown). The two species of echinoderm sperm were morphologically indistinguishable after Hepes-NaCl treatment. Other features of the sperm cells illustrated in Fig. 3 a are a portion of the mitochondrion (M) showing quite clear membrane structures, and microtubules (mt) associated with the axoneme.

To obtain preparations fully representative of the native state of the chromatin, living sperm were frozen in seawater. As expected, the vitreous state was not attained in the seawater medium, which contained hexagonal ice and sectioned poorly. However, the sperm themselves were often adequately frozen, as shown by electron diffraction patterns. Fig. 4 a shows an Epon section of portion of a GA-fixed *P. miniata* sperm cell, illustrating the closely packed chromatin fibers that are observed in conventional sections. Within the nucleus, well-resolved fibers are confined to regions where fibers are sectioned in a favorable orientation. Close to the nuclear periphery, fibers tend to run parallel to each other, and extended regions showing longitudinal views are common (Fig. 4 a, arrowheads). A similar effect is seen in frozen hydrated sections of unfixed whole cells (Fig. 4 b-d). Longitudinal views of chromatin fibers are seen occasionally, and they occur principally toward the nuclear envelope. Where individual fibers are clearly resolved (bracketed regions in Fig. 4 b-d), they have a uniform diameter. In other places,

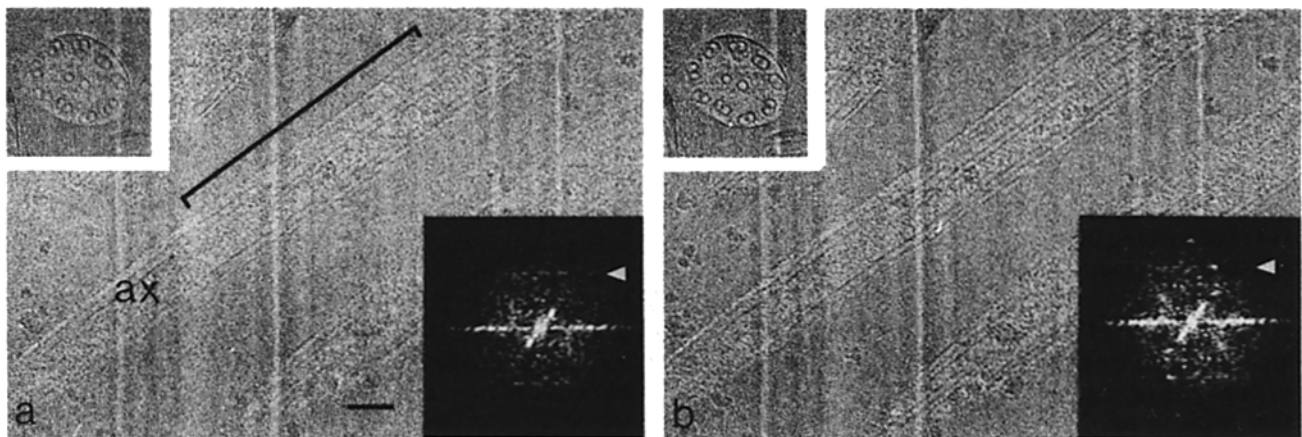


Figure 2. Image quality in frozen hydrated sections. A section containing axonemes cut longitudinally (ax) and transversely (top left insets) is shown at a nominal defocus of 2 (a) and 4 μm (b). Power spectra of the region of axoneme denoted by the bracket in a are shown at bottom right. In both cases, a prominent layer line at 1/8.8 nm is present (arrowheads), and information extends to at least 5 nm. Vertical lines on the sections are knifemarks which mark the cutting direction. Bar, 100 nm.

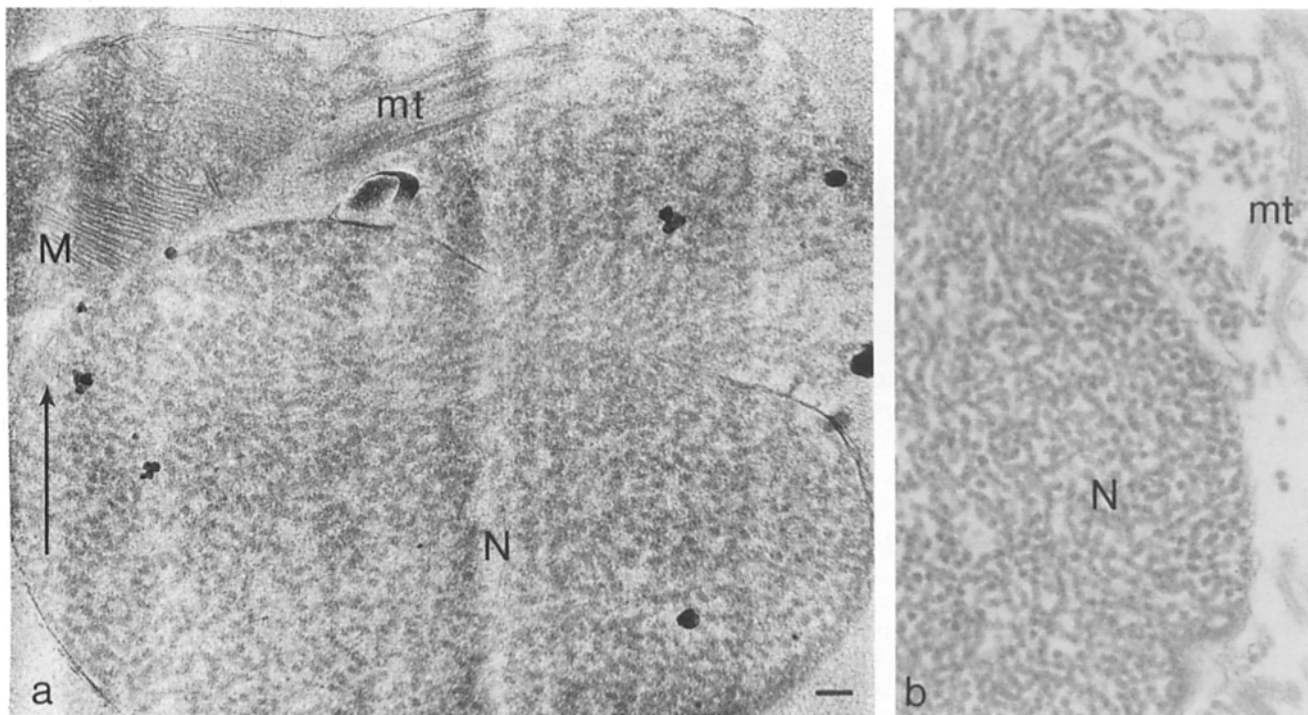


Figure 3. (a) Frozen hydrated section of sperm nucleus of *T. briareus* after exposure to Hepes-NaCl as described in the text, and cryoprotection with 15% dextran. The swollen nucleus (*N*) is filled with chromatin fibers, some of which are spilling out of the nuclear envelope. Also seen are portions of the microchondrion (*M*) and microtubules (*mt*) associated with the flagellar apparatus. Large arrow indicates the direction of sectioning. Nominal defocus = 4 μm . (b) Similar sample as in *a*, but after glutaraldehyde fixation and epoxy embedding. The nucleus and chromatin fibers appear very similar to the frozen hydrated condition. Bar, 100 nm.

it is clear that the chromatin consists of fibers (e.g., Fig. 4 *b*, arrowheads), but individual fibers are not sufficiently well separated to make reliable diameter measurements possible. These images from cells that were swimming in seawater until the moment of cryo-immobilization illustrate the native condition of the nuclei and provide a "baseline" against which the effects of all other treatments may be judged.

When *T. briareus* sperm are fixed in seawater and embedded in epoxy resin, chromatin fibers are more closely packed than in *P. miniata* (not shown), and difficult to resolve. Due to the very close packing, fibers were not seen in *T. briareus* sperm that had been frozen in seawater. Another feature of cryosections illustrated in Fig. 4, *b* and *d* is the "bubbling" effect of beam damage. In the absence of cryoprotectant, the sections are particularly sensitive to electrons, and "bubbles" tend to nucleate along the knife marks (Fig. 4 *b*, black dots). Repeated exposure of the same area increases the size and number of bubbles, but in regions free of bubbles chromatin fibers show no changes in structure or diameter.

Chromatin Fiber Morphology and Ultrastructure

Chromatin fibers have been examined closely both in the native close-packed state (Fig. 4) and the more dispersed condition (Figs. 3 and 5). In both cases, they are relatively smooth in outline, showing no signs of a discontinuous "supranucleosomal" organization (e.g., Zentgraf and Franke, 1984). Little structural detail can be seen within the frozen hydrated chromatin fibers. As with the axonemal microtubules, the fibers become visible at a nominal defocus level of about

2 μm , at which point there is little internal texture (Fig. 5). As the defocus is increased, a granular texture emerges that becomes progressively coarser, but is shared by the external medium and other cell components, and does not appear to be related to the imaging of individual nucleosomes. Throughout the focal range in which fibers are visible, there is no change in density between the center and periphery of the fibers, and computed diffraction patterns show no evidence of internal symmetry or regularity.

Chromatin Fibers in Chicken Erythrocyte Nuclei

Chicken erythrocyte nuclei were vitrified under conditions shown previously to be advantageous for observing chromatin fibers and to retain the fiber diameter observed in whole cells (Horowitz et al., 1990). Fig. 6 shows a frozen section in which portions of two nuclei (*N*) are present. Since the nuclei are prepared using detergent, the nuclear membrane is absent, and the nuclear periphery (Fig. 6, arrowheads) rather indistinct. A small amount of beam-induced bubbling is present, especially at the nuclear periphery. Within these unfixed nuclei, chromatin fibers are clearly visible (Fig. 6), and are similar in morphology and ultrastructure to those observed in the echinoderm sperm nuclei. Erythrocyte nuclei isolated under these conditions have numerous adhering intermediate filaments (Woodcock, 1980); these are visible also in frozen sections (Fig. 6). In the few experiments carried out on whole chicken erythrocytes, the vitreous state was rarely achieved.

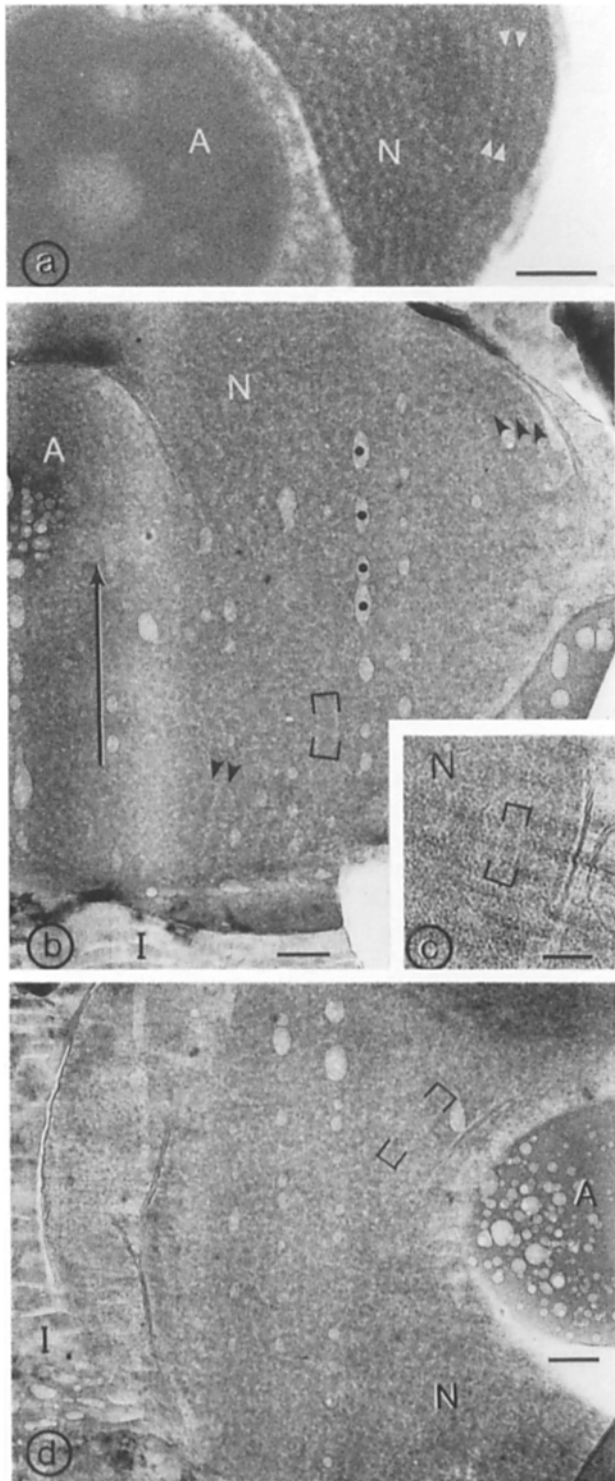


Figure 4. (a) Portion of a *P. miniata* sperm cell after GA fixation in seawater and embedding in Epon. In favorably oriented regions (white arrowheads), chromatin fibers are seen in longitudinal view lying parallel to the nuclear envelope. Closer to the acrosome (A) is a group of fibers cut obliquely. (b–d) Cryosections of whole *P. miniata* sperm after freezing in seawater. The seawater medium contains crystalline ice (I) and sections poorly, but the cells give satisfactory sections. Within the nuclei (N) there are several places where close-packed chromatin fibers are evident. Some fibers, such as those within the bracketed regions are sufficiently well-defined to allow diameter measurements to be taken. In other regions

Chromatin Fiber Diameter

Because of the significance of chromatin fiber diameter for models of chromatin architecture, and the issue of the observed differences in diameter between isolated and in situ fibers (Giannasca et al., 1993), an important goal of this study was to obtain accurate diameter measurements from the frozen hydrated sections.

A complication in taking measurements from frozen sections is that they are compressed during cutting (Dubochet et al., 1988). This effect, clearly seen in Fig. 3, results in a concomitant increase in section thickness but not a lateral expansion. The following strategy was used to compensate for compression. First, for each nucleus, measurable regions of fiber were identified. These were lengths of well-defined fiber that were straight for at least 150 nm (e.g., Figs. 5 and 6, black lines). Both the diameter and the angle (α) of each fiber segment with respect to the knife marks on the section were then measured. In some nuclei, there were at least 15 fiber segments that were parallel ($\pm 5^\circ$) with the knife marks, and for which the diameters should not be affected by compression. For nuclei in which fewer fibers had this orientation, plots of diameter versus $\text{Cos}(\alpha)$ were prepared and linear regression values calculated (Fig. 7). The graphs support a linear relationship between diameter and $\text{Cos}(\alpha)$ (r^2 values for the regression ranged from 0.5 to 0.7), confirming that compression is a simple unidirectional phenomenon. On the graphs, the intercepts of the regression lines on the y-axis yield the real diameter (fiber parallel to knife marks, diameter not affected by compression) and the minimum diameter (fiber perpendicular to knife marks, diameter maximally affected by compression). The ratio of maximum to minimum diameter gives the compression factor, which ranged from 25 to 30%, in agreement with previous estimates (Dubochet et al., 1988). There was no significant difference ($P > .05$) between diameters determined exclusively from uncompressed fiber segments (parallel to knife marks) and diameters obtained using the regression method.

The effect on diameter measurements of the defocus needed to obtain adequate contrast was also investigated. Measurements were taken from epoxy sections at 0, 2, and 4 μm defocus, and from frozen sections at 2, 4, and 6 μm defocus. The results showed that underfocussing to 4 μm produced an overestimate of diameter not exceeding 1.5 nm, a value consistent with the simulations of Athey et al. (1990).

The results of the fiber diameter measurements from frozen hydrated sections, together with compilations from previous work on sections and on isolated chromatin fibers, are shown in Table I. For frozen hydrated sections, the most notable feature is the similarity in mean diameter both between treatments and between species. Neither glutaraldehyde fixation nor the Hepes-NaCl treatment used to effect fiber dispersion has a significant ($P > .05$) effect on fiber di-

(black arrowheads), a “fiber morphology” is evident, but individual fibers are not suitable for measurement. Beam damage in the form of “bubbles” initiates along knife marks in nuclei (b, dots), and more generally in the acrosomes (A). The arrow in b denotes the direction of sectioning. Nominal defocus is 2 μm for b and d, 4 μm for c. All scale bars are 100 nm. Note that a has been printed at a magnification approximately 25% greater than b–d in order to provide a better visual comparison.

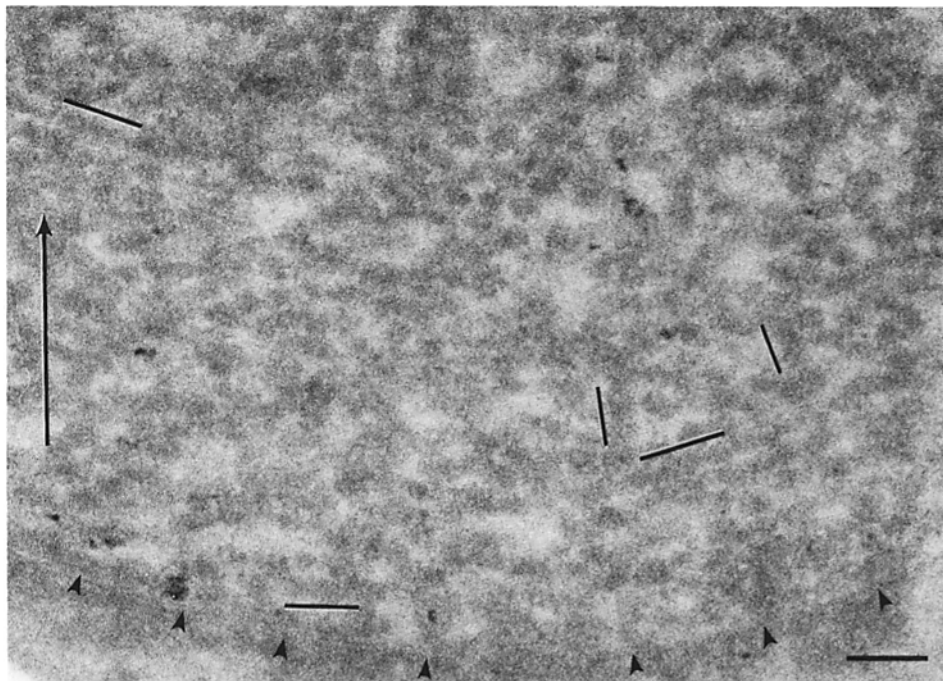


Figure 5. Higher magnification view of a frozen hydrated section of *P. miniata* sperm after Hepes-NaCl treatment. Chromatin fibers show little internal structure. Lines have been placed alongside fibers suitable for diameter measurements. The effect of cutting direction (*arrow*) on fiber diameter is evident: the two fibers that are nearly parallel to the direction of cutting are wider than the other three. Arrowheads indicate the position of the nuclear envelope. Nominal defocus = 2 μm . Bar, 100 nm.

ameter. Moreover, there is clearly no evidence for a positive correlation between fiber diameter and nucleosomal repeat length. The only significant ($.01 < P < .05$) between species diameter difference is for *P. miniata* and *T. briareus* recorded after fixation in Hepes-NaCl, and this difference is contrary to that predicted on the basis of nucleosome repeat length. There is, however, good agreement between diameter values

obtained from cryosections and from low temperature embeddings in Lowicryl K11M. Indeed, apart from the exception mentioned above (*P. miniata* and *T. briareus* sperm fixed in Hepes-NaCl), there are no significant differences ($P > .05$) between diameters obtained with either low temperature technique under any of the pre-treatment conditions.

In contrast, diameters of isolated chromatin fibers of both

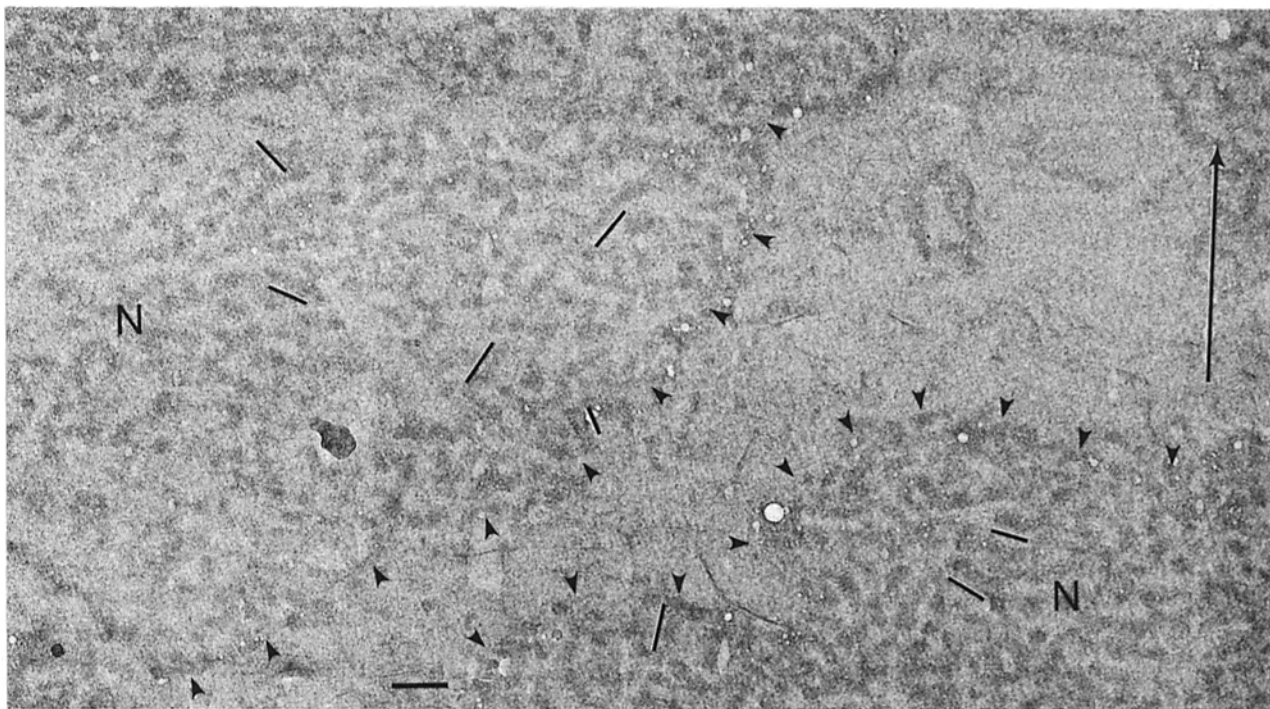


Figure 6. Frozen hydrated section of isolated chicken erythrocyte nuclei (*N*), the edges of which have been marked by arrowheads. The nuclear interiors contain a mass of chromatin fibers, some of which are suitable for diameter measurement (*lines*). Intermediate filaments are seen between the nuclei. Large arrow shows sectioning direction. Nominal defocus = 4 μm . Bar, 100 nm.

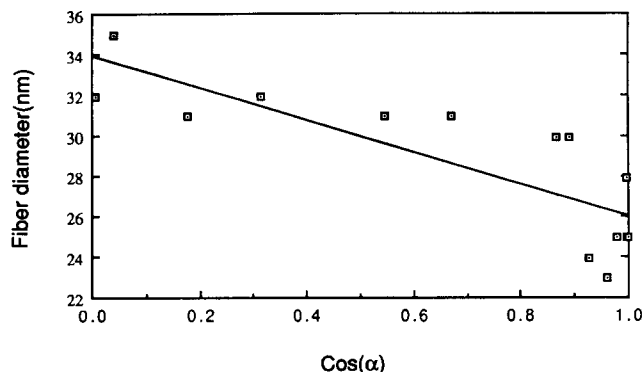


Figure 7. Graph of fiber diameter against $\text{Cos}(\alpha)$ where (α) is the angle between the fiber segment and the direction of cut. Also shown is the calculated linear regression line. For this data set $r^2 = 0.67$. The intercepts of linear regression line on the y-axis allow the compression to be estimated (see text).

P. miniata after negative staining (Giannasca et al., 1993) and *T. briareus* in frozen hydrated or negatively stained preparations (Athey et al., 1990; Williams et al., 1986) are 8–10-nm larger than the in situ values recorded from cryosections. Diameter measurements reported for isolated chicken erythrocyte chromatin fibers have been very variable, ranging from 22 nm (Ruiz-Carrillo et al., 1980) to 38 nm (Woodcock et al., 1984). This may be due to the sensitivity of this material to the ionic composition of the medium (Woodcock et al., 1984; Alegre and Subirana, 1989). Because of this uncertainty, no meaningful comparisons between the isolated and in situ fiber diameters of chicken erythrocyte chromatin can yet be made.

Fiber diameters measured in epoxy sections are 6–10-nm smaller than with low temperature methods (Table I). This is consistent with the ~25% shrinkage recorded during con-

ventional epoxy embedding of nuclei (Langmore and Paulson, 1983). It has been our experience, moreover, that the extent of epoxy shrinkage varies greatly from experiment to experiment. A graphic example of epoxy-induced shrinkage is seen in Fig. 4, where the epoxy section (Fig. 4 a) has been printed at a 25% higher magnification than the frozen hydrated sections in Fig. 4 (b–d) in order to provide a useful visual comparison.

Variability of Fiber Diameter

As seen from the standard deviations in Table I, which are typically 7 to 10% of the mean values, fiber diameter measurements within a single treatment are quite variable. In contrast, the standard deviation for microtubules in the same sections is typically less than 5% of the mean. A similar effect was noted by Athey et al. (1990) for the diameter of isolated chromatin fibers. These authors also measured the diameter of tobacco mosaic virus particles in the same preparations, and found that the standard deviation for this material was only 5% of the mean. As suggested by Athey et al. (1990), the wider spreads of fiber diameter values appear to reflect a true variability in chromatin structure, rather than an increased measuring error.

Discussion

For material that can be vitrified in the living state, without recourse to cryoprotection or fixation, frozen hydrated sections provide the closest approach to the native ultrastructure. Echinoderm sperm can be vitrified while swimming in seawater (Fig. 4, a and b), and this property allows the native ultrastructure of the chromatin of these cells to be examined. Because of the low contrast of unstained frozen hydrated sections, the information recorded in micrographs is strongly dependent on the imaging conditions, especially the level of

Table I. Diameter of Chromatin Fibers in Sections and after Isolation

Source linker DNA length [§]	Fiber diameter (nm)		
	Chicken erythrocyte ~66 bp	<i>P. miniata</i> sperm ~76 bp	<i>T. briareus</i> sperm ~86 bp
Frozen hydrated sections			
Seawater, unfixed	nf*	34.3 SD 1.7 n = 11 [‡]	nf*
Hepes-NaCl, unfixed	33.3 SD 2.6 n = 15 [‡]	33.2 SD 4.5 n = 20	32.4 SD 1.7 n = 7 [‡]
Hepes-NaCl, fixed	31.0 SD 2.2 n = 14 [‡]	34.7 SD 2.4 n = 19 [‡]	32.5 SD 2.6 n = 15
	ND	36.5 SD 2.9 n = 19 [‡]	33.2 SD 2.3 n = 18
			33.1 SD 2.2 n = 14 [‡]
Mean of means	32.2	34.4	34.0 SD 2.1 n = 14 [‡]
Lowicryl sections	31.2 SD 2.0	31.0 SD 2.1 [†]	33.0
Epon sections	23.5 SD 3.4	26.4 SD 3.0 n = 14	27.4 SD 1.7 n = 16
Isolated fibers	32.0 SD 8.0 ^{**}	42.0 SD 2.0 ^{‡‡}	43.5 SD 4.2 ^{‡‡}

All values from this study except as indicated. In cases where there are more than one entry in a column, each value represents an independent determination.

* No fibers seen

[‡] Determined from regression line (see text)

[§] Nucleosomal repeat minus 146 bp

^{||} From Horowitz et al. (1990)

[†] From Horowitz and Woodcock (1992)

^{**} From Woodcock et al. (1984) (fibers in 20 mM NaCl)

^{‡‡} From Giannasca et al. (1993)

^{‡‡} From Athey et al. (1990)

ND, Not determined

defocus. By recording images at two or more defocus levels, the possibility of missing, or wrongly interpreting structural features was minimized. Under the imaging conditions used here, positive findings, such as the presence and general morphology of chromatin fibers can be accepted with confidence. The failure to resolve individual nucleosomes within chromatin fibers is probably related to the inherent lack of contrast between unstained DNA and protein: with Lowicryl embedded nuclei, DNA-specific staining is required to resolve nucleosomes (Horowitz and Woodcock, 1992).

Presence of Chromatin Fibers In Vivo

The native state of chromatin in *P. miniata* sperm is close-packed chromatin fibers (Fig. 4) with an intra-nuclear distribution and general morphology similar to that seen in conventional sections (Giannasca et al., 1993). MacDowall et al. (1986), finding no evidence for chromatin fibers in frozen hydrated sections of CHO and HeLa cell chromosomes, suggested that chromatin exists in a "liquid" state, the individual nucleosomes having sufficient thermal mobility to preclude the presence of fibers. As discussed below, the liquid model may be a useful concept for nuclei in which fibers are not observed in conventional or frozen hydrated sections. However, the present cryosection results show that "30-nm" fibers do indeed constitute the native conformation of certain chromatin.

Having established a baseline nuclear ultrastructure with unfixed frozen hydrated sections, it is possible to determine the effects of fixation, dehydration, and embedding. The close correspondence in nuclear ultrastructure and fiber morphology between frozen hydrated preparations made before and after glutaraldehyde crosslinking indicates that, to the level of resolution achieved in these cryosections, glutaraldehyde produces no structural changes. It is also clear that low temperature embedding in Lowicryl following glutaraldehyde fixation preserves both fiber morphology (Horowitz and Woodcock, 1992) and diameter (Table I). These findings will allow future work on nuclear ultrastructure using glutaraldehyde fixation and Lowicryl embedding to be interpreted without the usual caveats about potential changes in structure during preparation.

Chromatin Fiber Diameter and Its Relation to Nucleosome Repeat Length

The presence of chromatin fibers in frozen hydrated nuclei made it possible to obtain measurements of fiber diameter that were not compromised by the effects of fixation, dehydration, or embedding. Fortunately, the compression that occurs during cryosectioning affects fiber diameter in a simple linear fashion and can be readily compensated (Fig. 7). Chromatin fiber diameter has become a particularly significant parameter for two reasons. First, for chromatin models in which the linker traverses the fiber, diameter is predicted to be proportional to linker length (Williams et al., 1986; Bordas et al., 1986). Second, recent results have suggested that, for starfish sperm chromatin, isolated fibers are significantly wider than those originally present in the nucleus (Giannasca et al., 1993).

Fiber diameter in the frozen hydrated starfish nuclei (Table I) was 34.3 nm (1.7 nm SD), slightly larger than the 31.0 nm (2.1 SD) found in low temperature embedded nuclei, but significantly ($P < .01$) smaller than the 42.0 nm (2.0 nm SD)

value obtained from isolated fibers (Giannasca et al., 1993). The alteration of chromatin fibers during the isolation process (Giannasca et al., 1993) is thus confirmed.

Table I also shows that, in the frozen hydrated material, there is no consistent relationship between fiber diameter and nucleosomal repeat length. This is contrary to findings based on isolated chromatin: Williams et al. (1986) and Athey et al. (1990) reported a strong positive correlation between fiber diameter and nucleosome repeat for isolated chromatin. The linear regression equation derived from their compiled data predicts a 2.4-nm diameter increase for a 10-bp increase in nucleosome repeat (Athey et al., 1990), and thus a ~ 5 nm difference between chicken erythrocyte (nucleosomal repeat ~ 212 bp) and *T. briareus* sperm chromatin (nucleosomal repeat ~ 235 bp). A difference of this magnitude is not observed in frozen hydrated sections (Table I), the discrepancy most likely being related to effects of the isolation process.

Alegre and Subirana (1989) have suggested a correlation between chromatin fiber diameter and nucleosome repeat length based on measurements taken from epoxy-embedded nuclei. As previously discussed (Giannasca et al., 1993), this study is largely focussed on the effects of salt concentration on fiber diameter, and the evidence supporting a relationship between diameter and nucleosomal repeat is not strong. Williams et al. (1986) obtained X-ray scattering data from isolated *T. briareus* nuclei and suggested that the "20-nm" feature in the X-ray profile resulted from the scattering of chromatin fibers as cylinders. Modeling based on this interpretation gave a fiber diameter of 39.4 nm, considerably larger than the frozen hydrated section measurements (Table I). The direct measurements reported here are free of assumptions and, at present, there appears to be no compelling evidence from earlier work using epoxy-embedded nuclei, or X-ray scattering, that native fiber diameters are correlated with nucleosome repeat length.

The lack of a positive correlation between fiber diameter and nucleosomal repeat is puzzling in view of our recent visualization of extended linker DNA in sections of low temperature embedded *P. miniata* sperm nuclei (Woodcock et al., 1993). These images suggest that linker DNA is not coiled between adjacent nucleosomes, as in "solenoid" models (Felsenfeld and McGhee, 1984). One possibility is that in vivo, fiber diameter is constrained within the nucleus, perhaps by soluble components such as ions or polyelectrolytes in the nuclear milieu. During chromatin isolation, the compact fiber morphology is lost (Giannasca et al., 1993), and the re-establishment of a fiber morphology in solution occurs without these constraints, leading to the observed relationship between diameter and linker DNA length.

Different States of Native Chromatin Conformation?

Cells may be classified into two categories on the basis of their nuclear ultrastructure: those in which "30-nm" chromatin fibers are readily seen in thin sections of whole cells, and those in which fibers are not clearly evident. The first category is largely confined to cells in which the chromatin is condensed, transcriptionally inactive, and has a long (>210 bp) nucleosome repeat. Included here are echinoderm sperm and avian erythrocytes. The second category comprises the majority of "typical" eukaryotic nuclei which have nucleosome spacings in the 160–200-bp range (van Holde, 1988).

In these nuclei, it is generally not possible to recognize chromatin fibers in frozen hydrated sections (Dubochet et al., 1988), low temperature embedded material (e.g., Horowitz et al., 1990), or conventional epoxy sections.

Until now, it has been possible to argue that the absence of "30-nm" fibers in the majority of nuclei was due to some failure to preserve them adequately, and that their absence in frozen hydrated sections (Dubochet et al., 1988; MacDowall et al., 1986) was the result of the poor contrast of unstained biological material in ice. With the observations of chromatin fibers in frozen hydrated nuclei presented here, these arguments are no longer tenable. The two categories of nuclear ultrastructure are not the result of a failure of the preservation or imaging methodology, but a valid reflection of differing states of chromatin conformation.

A clear example of a naturally occurring transition in chromatin conformation is that of sperm development in the echinoderm *Strongylocentrotus purpuratus*. Spermatogonia have nuclei that show a discrimination between condensed heterochromatin and dispersed euchromatin, but do not contain chromatin fibers, while spermatid nuclei are filled with uniformly distributed "30-nm" fibers (Ward and Nishioka, 1993). Interestingly, in this species, a further compaction occurs in the mature sperm, where chromatin fibers are again absent. Such developmental changes are associated with an increase in nucleosomal repeat, reduction in non-histone chromosomal proteins, and appearance of new species of very lysine rich histones (Poccia et al., 1989). Chromatin transitions may also be effected experimentally. Isolated chromatin assumes a "30-nm" fiber conformation under appropriate salt conditions even when extracted from nuclei in which fibers were absent (e.g., Thoma et al., 1979), and the exposure of nuclei or chromosomes to a brief reduction in ionic strength often results in the appearance of fibers (e.g., Alegre and Subirana, 1989; Kirschner et al., 1977; Bahr, 1977).

It is now appropriate to revise the paradigm of the "30-nm" chromatin fiber as a single universal structure adopted by inactive genes in vivo and after isolation, and recognize the true complexity of the situation. Recent tomographic three dimensional reconstructions show that even in nuclei with clearly defined chromatin fibers there are regions where fibers interdigitate with each other and lose their individuality (Horowitz et al., 1994). A more extensive interdigitation could lead to the fiber-less morphology of condensed chromatin in "typical" nuclei and chromosomes, and be consistent with the fluid type of organization suggested by MacDowall et al. (1988). The absence of chromatin fibers from most nuclei further suggests that the accessibility of genes in condensed chromatin to transcriptional regulators is not a function of the specific architecture of a canonical "30-nm" fiber.

I thank Dr. J. Dubochet for his generosity in providing the facilities for this work and for his help and encouragement, Mme L. Salamin-Michel for assistance with cryotechnique, Mme. J. Fakan for epoxy embedding and sectioning, and Ms. R. A. Horowitz for valuable comments on the manuscript.

Supported in part by Fogarty Senior Fellowship TW-01818 and National Institutes of Health GM-43786.

Received for publication 22 November 1993 and in revised form 11 January 1994.

References

- Alegre, C., and J. A. Subirana. 1989. The diameter of chromatin fibres depends on linker length. *Chromosoma*. 98:77-80.
- Athey, B. D., M. F. Smith, S. P. Williams, D. A. Rankert, and J. P. Langmore. 1990. The diameters of frozen-hydrated Thyone and Necturus chromatin fibers increase with DNA linker length: evidence in support of variable diameter models for chromatin. *J. Cell Biol.* 111:795-806.
- Bahr, G. F. 1977. Chromosomes and Chromatin Structure. In *Molecular Structure of Human Chromosomes*, J. J. Yunis, editor. Academic Press, New York: 144-204.
- Bordas, J., L. Perez-Grau, M. H. J. Koch, M. C. Vega, and C. Nave. 1986. The superstructure of chromatin and its condensation mechanism II: theoretical analysis of the X-ray scattering patterns and model calculations. *Eur. J. Biophys.* 13:175-185.
- Davies, H. G., A. B. Murray, and M. E. Walmsley. 1974. Electron microscope observations on the organisation of the nucleus in chicken erythrocytes and a superunit thread hypothesis for chromosome structure. *J. Cell Sci.* 16:261-299.
- Dubochet, J., M. Adrian, J. J. Chang, J. C. Homo, J. Lepault, A. W. McDowall, and P. Schultz. 1988. Cryo-electron microscopy of vitrified specimens. *Q. Rev. Biophys.* 21:129-228.
- Felsenfeld, G., and J. D. McGhee. Structure of the 30 nm chromatin fiber. *Cell*. 44:375-377.
- Erikson, H. P., and A. Klug. 1971. Measurement and compensation of defocussing and aberrations by Fourier processing of electron micrographs. *Phil. Trans. Roy. Soc. Lond. B* 261:105-118.
- Frank, J., B. Shimkin, and H. Dowse. 1981. SPIDER—a modular software system of electron microscopy and image processing. *Ultramicroscopy*. 6: 343-358.
- Giannasca, P. J., R. A. Horowitz, and C. L. Woodcock. 1993. Transitions between in situ and isolated chromatin. *J. Cell Sci.* 105:551-561.
- Horowitz, R. A., P. J. Giannasca, and C. L. Woodcock. 1990. Ultrastructural preservation of nuclei and chromatin: Improvement with low-temperature methods. *J. Microsc.* 157:205-224.
- Horowitz, R. A., D. A. Agard, J. W. Sedat, and C. L. Woodcock. 1994. The 3D architecture of chromatin fibers in situ. Electron tomography reveals an architecture based on a continuously variable zig-zag ribbon. *J. Cell Biol.* 125:1-10.
- Horowitz, R. A., and C. L. Woodcock. 1992. Alternative staining methods for low cryo sections. *J. Histochem. Cytochem.* 40:123-133.
- Kirschner, R. H., M. Rusli, and T. E. Martin. 1977. Characterization of the nuclear envelope, pore complexes, and dense lamina of mouse liver nuclei by high resolution scanning electron microscopy. *J. Cell Biol.* 72:118-132.
- Langmore, J. P., and J. R. Paulson. 1983. Low angle x-ray diffraction studies of chromatin structure in vivo and in isolated nuclei and metaphase chromosomes. *J. Cell Biol.* 96:1120-1131.
- McDowall, A. W., J. M. Smith, and J. Dubochet. 1986. Cryo-electron microscopy of vitrified chromosomes in situ. *EMBO (Eur. Mol. Biol. Organ.) J.* 5:1395-1402.
- Murray, J. M. 1986. Electron microscopy of frozen hydrated eukaryotic flagella. *J. Ult. Mol. Struct. Res.* 95:196-209.
- Poccia, D. L., M. V. Simpson, and G. R. Green. 1987. Transitions in histone variants during sea urchin spermatogenesis. *Dev. Biol.* 121:445-453.
- Rattner, J. B., and B. A. Hamkalo. 1978. Higher order structure in metaphase chromosomes. *Chromosoma*. 69:363-379.
- Ruiz-Carrillo, A., P. Puigdomenech, G. Eder, and R. Lurz. 1980. Stability and reversibility of higher ordered structure of interphase chromatin: continuity of deoxyribonucleic acid is not required for maintenance of folded structure. *Biochemistry*. 19:2544-2554.
- Stewart, M. 1989. Transmission electron microscopy of frozen hydrated biological material. *Electron Microsc. Rev.* 2:117-121.
- Thoma, F., T. Koller, and A. Klug. 1979. Involvement of histone H1 in the organization of the nucleosome and of the salt-dependent superstructures of chromatin. *J. Cell Biol.* 83:403-427.
- Tilney, L. G. 1986. The polymerization of actin II. *J. Cell Biol.* 69:51-72.
- van Holde, K. E. 1988. Chromatin. Springer-Verlag, New York.
- Ward, R. D., and D. Nishioka. 1993. Seasonal changes in testicular structure and localization of a sperm surface glycoprotein during spermatogenesis in sea urchins. *J. Histochem. Cytochem.* 41:423-431.
- Williams, S. P., B. D. Athey, L. J. Muglia, R. S. Schappe, A. H. Gough, and J. P. Langmore. 1986. Chromatin fibers are left-handed helices with diameter and mass per unit length that depend on linker length. *Biophys. J.* 49:233-248.
- Woodcock, C. L. F. 1980. Nucleus-associated intermediate filaments from chicken erythrocytes. *J. Cell Biol.* 85:881-889.
- Woodcock, C. L. F., L.-L. Y. Frado, and J. B. Rattner. 1984. The higher order structure of chromatin: evidence for a helical ribbon arrangement. *J. Cell Biol.* 99:42-52.
- Woodcock, C. L., S. A. Grigoryev, R. A. Horowitz, and N. Whitaker. 1993. A chromatin folding model that incorporates linker variability generates fibers resembling the native structures. *Proc. Natl. Acad. Sci. USA.* 90: 9021-9025.
- Zentgraf, H., and W. W. Franke. 1984. Differences of supranucleosomal organization in different kinds of chromatin: cell type-specific globular subunits containing different numbers of nucleosomes. *J. Cell Biol.* 99:272-286.